

Low-Level Nuclear Activity in Nearby Spiral Galaxies

Himel Ghosh and Smita Mathur

*Department of Astronomy, The Ohio State University
140 W 18th Ave, Columbus, OH 43210*

ghosh,smita@astronomy.ohio-state.edu

Fabrizio Fiore

*INAF - Osservatorio Astronomico di Roma
via Frascati 33, 00040 Monteporzio Catone (Roma), Italy*

fiore@oa-roma.inaf.it

and

Laura Ferrarese

*Herzberg Institute of Astrophysics
5071 West Saanich Road, Victoria, BC V8X 4M6, Canada*

laura.ferrarese@nrc-cnrc.gc.ca

ABSTRACT

We are conducting a search for supermassive black holes (SMBHs) with masses below $\sim 10^7 M_\odot$ by looking for signs of extremely low-level nuclear activity in nearby galaxies that are not known to be AGNs. Our survey has the following characteristics: (a) X-ray selection using the *Chandra* X-ray Observatory, since x-rays are a ubiquitous feature of AGNs; (b) Emphasis on late-type spiral and dwarf galaxies, as the galaxies most likely to have low-mass SMBHs; (c) Use of multiwavelength data to verify the source is an AGN; and (d) Use of the highest angular resolution available for observations in x-rays and other bands, to separate nuclear from off-nuclear sources and to minimize contamination by host galaxy light. Here we show the feasibility of this technique to find AGNs by applying it to six nearby, face-on spiral galaxies (NGC 3169, NGC 3184, NGC 4102, NGC 4647, NGC 4713, NGC 5457) for which data already exist in the *Chandra* archive. All six show nuclear x-ray sources. The data as they exist at present are ambiguous regarding the nature of the nuclear x-ray sources in NGC

4713 and NGC 4647. We conclude, in accord with previous studies, that NGC 3169 and NGC 4102 are almost certainly AGNs. Most interestingly, a strong argument can be made that NGC 3184 and NGC 5457, both of type Scd, host AGNs.

Subject headings: galaxies:active—galaxies:nuclei—galaxies:spiral

1. Introduction

The past decade has seen extraordinary improvement in our understanding of super-massive black holes (SMBHs) — their growth and evolution, and their links with their host galaxies. We now realize that galaxies hosting SMBHs at their centers are the rule rather than the exception. The observed correlations of the masses M_\bullet of the SMBHs with properties of their host galaxies, for example with the bulge stellar velocity dispersion (Ferrarese & Merritt 2000; Gebhardt et al. 2000), show that there is a close link between the formation and evolution of galaxies and of the SMBHs they host. Furthermore, a comparison of the SMBH mass function required to explain the observed luminosity function of active galactic nuclei (AGNs) with estimates of the local SMBH mass function (e.g. Marconi et al. 2004; Shankar et al. 2004) shows that not only do all galaxies have SMBHs, but that these black holes are AGN relics. Thus knowledge of the local SMBH mass function enables us to put constraints on theories of galaxy and SMBH formation and growth, and AGN lifetimes.

Estimates of the local SMBH mass function are anchored by direct, dynamical measurements of the masses of ~ 30 SMBHs, and otherwise based on the distribution of host galaxy properties (luminosity of the bulge or bulge stellar velocity dispersion σ) and known scaling relationships between the mass of the SMBH and these properties (most prominently $M_\bullet - \sigma$ and $M_\bullet - M_{\text{bulge}}$). Most of the measured SMBH masses are $\sim 10^8 M_\odot$ or greater, however, as the sphere of influence of a less massive SMBH is extremely hard to resolve even at moderate distances, even with *HST*. For example, the sphere of influence of a $10^6 M_\odot$ SMBH at 15 Mpc is ~ 30 milliarcseconds (mas). As a result, while different estimates of the mass function agree at the high-mass end, the low-mass end ($M_\bullet \lesssim 10^6 M_\odot$) often has discrepancies (see, e.g., Fig. 7 of Graham et al. 2007, for a comparison of different authors' estimates of the mass function). A second source of uncertainty at the low-mass end is the fact that it is unknown how the scaling relationships extrapolate to very late-type spiral galaxies, which have little or no bulge component, and to very low mass galaxies (dE and dSph). Yet SMBHs *do* exist in very late-type spirals, e.g. NGC 4395, a spiral galaxy of type Sdm, with $M_\bullet \sim 3 \times 10^5 M_\odot$ (Peterson et al. 2005), and in very low mass galaxies, e.g. POX 52, a dwarf galaxy, with $M_\bullet \sim 3 \times 10^5 M_\odot$ (Barth et al. 2004). Questions that naturally arise

at this point are: Do the scaling relationships break down at low masses? What determines the mass of an SMBH: the mass of the bulge or the mass of the dark matter halo? Is there a lower bound to the local SMBH mass function? A well defined sample of low-mass SMBHs is needed to answer these questions.

Since we cannot detect low-mass SMBHs by their dynamical signature, looking for them by signs of their accretion activity may be the only viable way of detecting them. This of course limits detection to the subset of low-mass black holes that are active, but this fraction can be expected to be large, for the following reason. We now understand that the “quasar era” is a function of luminosity, with the space density of the most luminous quasars peaking at high redshift and that of lower luminosity quasars peaking at progressively lower redshifts (Fiore et al. 2003; Hasinger et al. 2005). This is often referred to as the “downsizing” of AGN activity with cosmic epoch. Moreover, it has also become clear that massive SMBHs did all their growing at high redshift while the lower-mass SMBHs grew at progressively lower redshifts, a phenomenon often referred to as “anti-hierarchical BH growth” (e.g. Merloni 2004). Therefore the lowest-mass SMBHs should still be accreting at the present epoch. The idea of looking for candidate low-mass SMBHs by signs of AGN activity was applied by Greene & Ho (2004) and Heckman et al. (2004), for example, where the particular AGN signature used was the presence of characteristic emission lines in the optical spectrum. A different signature that can be used is x-ray emission. X-ray emission is a ubiquitous feature of active galaxies. In a search for extremely low luminosity AGN, x-ray selection has some advantages over spectroscopic selection. First, x-rays can penetrate obscuring material which may be hiding the line emitting regions. Second, there are fewer sources of x-rays in a galaxy than there are of optical and UV emission and so dilution of the AGN signature by host galaxy light is less of a problem. Where the luminosity of the AGN is low to begin with, even a modest amount of absorption may result in the signal being below the optical background imposed by the galaxy. Third, even if, as expected in some theories (Eracleous et al. 1995; Nicastro 2000; Nicastro et al. 2003; Laor 2003) AGNs that have luminosities or accretion rates below a cut-off value do not have broad-line regions, they should still be detectable in x-rays. X-ray observations have in fact detected AGNs in what were thought to be “normal” galaxies (e.g. Martini et al. 2002). The disadvantage, as discussed later in the paper, is that x-ray observations by themselves cannot always distinguish between AGNs and other x-ray sources, such as x-ray binaries (XRBs) and ultraluminous x-ray sources (ULXs). Multi-wavelength data are needed to determine the type of source.

As the first step towards assembling a sample of low-mass SMBHs, we are conducting an x-ray survey of nearby (within 20 Mpc), *quiescent* spiral galaxies using the *Chandra* X-ray Observatory to look for nuclear x-ray sources, with an emphasis on late-type spirals. The high angular resolution of *Chandra* is necessary to ensure that any detected source is really

at the center and is not an off-nuclear source. The survey is sensitive to an (unobscured) SMBH of mass $M_{\bullet} = 10^4 M_{\odot}$ radiating at $\sim 2 \times 10^{-3} L_{\text{Edd}}$ out to the survey limit. We will present details of the survey sample selection and the *Chandra* observations in a future paper. Here, we present the methods used and the feasibility of detecting AGNs using these methods by applying them to six galaxies that meet selection criteria similar to those used for the survey sample, and for whom x-ray data already exist in the *Chandra* archive.

The paper is organized as follows: §2 describes the criteria used to select the six galaxies presented here; §3 describes the observations and data analysis, with individual targets discussed in §§3.1–3.6; the results are discussed in §4.

2. Sample selection

Starting with Third Reference Catalogue of Bright Galaxies¹ (RC3; de Vaucouleurs et al. 1991), we imposed the following main filters. (1) Morphological type: we selected spiral galaxies of type Sa through Sd ($1.0 \leq T \leq 7.0$); (2) Distance: galaxies that had recession velocity $cz \leq 3000 \text{ km s}^{-1}$; (3) Galactic latitude: $|b| \geq 30^\circ$ to avoid x-ray absorption by gas in our own Galaxy; (4) Inclination: we required $\log(a/b) \leq 0.4$, where a and b are the projected lengths of the semi-major and semi-minor axes, respectively. This was to avoid obscuration by the disk of the host galaxy; (5) Nuclear inactivity: the galaxy must *not* be known to be an AGN or starburst. Starbursts were excluded since the vigorous star formation also increases the likelihood of the presence of XRBs and ULXs. LINERs were included as there is still debate about whether the fundamental source of energy in these nuclei is an AGN or star formation. We also required that the object have the value of the “goodposition” flag set to 1 in the RC3 table in the Sloan Digital Sky Survey (SDSS) database, which indicated that the coordinates of the galaxy were accurate to 0.1 s in RA and 1'' in Dec. All objects passing these filters were cross-correlated with SDSS Data Release 3, with a match radius of 30''. This resulted in a list of 104 galaxies. This list was then checked against publicly available data in the *Chandra* archive. The final sample consists of six galaxies: NGC 3169 (Sa), NGC 3184 (Scd), NGC 4102 (Sb), NGC 4647 (Sc), NGC 4713 (Sd), and NGC 5457 (Scd).

¹In practice, we accessed the RC3 table in the SDSS database.

3. Data analysis

Details of the observations that were analyzed are given in Table 1. X-ray data were downloaded from the *Chandra* archive and analyzed using version 3.4 of *Chandra* Interactive Analysis of Observations (CIAO) software. In each case the Level 2 event list was processed using the observation-specific bad-pixel file and the latest calibration files, and filtered to exclude times when the instrument experienced a background flare. The event lists were then converted to FITS images and the CIAO wavelet source detection tool *wavdetect* was run on them to determine source positions. For each observation, source counts were extracted from a circle centered on the *wavdetect* source position, and with a radius equal to the greater of 4.67 pixels (2.3'') and the 95% encircled-energy radius at 1.5 keV on ACIS-S at the position of the source. Background counts were taken from an annulus with an inner radius of twice, and an outer radius of five times, the source circle radius after excising any sources that happened to fall in the background region. Counts were extracted in the 0.3 – 8.0 keV (Broad), 2.5 – 8.0 keV (Hard) and 0.3 – 2.5 keV (Soft) bands. A hardness ratio (HR) was defined as $HR = (H - S)/(H + S)$, where H and S are the counts in the hard and soft bands, respectively. Spectral fits were performed with the CIAO tool *Sherpa*. Uncertainties reported in fit values represent the 90% confidence level for one parameter. In all estimations of the AGN Eddington ratio we have assumed that the bolometric luminosity is ten times the 2–10 keV luminosity of the AGN.

Where available, HST data were downloaded from the archive and analyzed using IRAF, essentially following the relevant Data Handbook provided by STScI. For ACS data, simple aperture photometry was done using the drizzled image, with the aperture matched to the source size. For WFPC2 data, background-subtracted source counts were determined using *imexam*, using a 2-pixel radius aperture for the source, and an annulus with an inner radius of 7 pixels and an outer radius of 12 pixels for the background. The counts were corrected for CTE effects using the method of Dolphin (2002) as implemented at the STScI website. The number of counts were then extrapolated to a 0.5'' radius aperture using the encircled-energy tables of Holtzman et al. (1995) and corrected for contamination of the CCD windows using *synphot* if necessary. This final number of counts and the values of the PHOTFLAM and PHOTZPT header keywords were then used to calculate the magnitude of the source in the STMAG system. A correction of -0.10 mag was added to represent the magnitude in an infinite aperture.

Individual targets are discussed below. For each target, we first describe the observed properties in the x-ray, and then in other wavebands when such observations exist. We then consider whether the evidence supports the hypothesis that the x-ray source is an AGN.

3.1. NGC 3169

This is a galaxy of type Sa, at a distance of 19.7 Mpc (Tully 1988), and its nucleus is classified as a LINER (Ho et al. 1997). The *Chandra* observation of the nucleus of NGC 3169 was analyzed by Terashima & Wilson (2003) and the nucleus identified as a low luminosity AGN, but the x-ray data are analyzed and presented here again for completeness. NGC 3169 was observed by *Chandra* for 2 ks and detected with 159 counts. Its hardness ratio $HR = +0.86$ makes it the hardest of the six sources discussed here and the only one to have a positive HR. Its spectrum, shown in Fig. 1, can be reasonably fit by an absorbed power-law, with $N_H \simeq 10^{23} \text{ cm}^{-2}$ and $\Gamma \simeq 2$. Spectral fit parameters are shown in Table 4, with the first row showing a fit using the Cash statistic and data binned to five counts per bin, and the second row a fit using the Gehrels χ^2 statistic and data binned by 20 PHA channels. Best-fit parameter values from both fits are consistent within errors with each other and with the results obtained by Terashima & Wilson (2003). Fluxes used in the analysis are from the Cash fit. The unabsorbed broad band flux is $f(0.3 - 8 \text{ keV}) = 1 \times 10^{-11} \text{ erg cm}^{-2} \text{ s}^{-1}$, implying a luminosity $L(0.3 - 8 \text{ keV}) = 5 \times 10^{41} \text{ erg s}^{-1}$ for the assumed distance.

Observations with the Very Large Baseline Array (VLBA) show the nucleus is a mas-scale radio source at 5 GHz (Nagar et al. 2005). The nuclear flux density is $f(5 \text{ GHz}) = 6.6 \times 10^{-26} \text{ erg cm}^{-2} \text{ s}^{-1} \text{ Hz}^{-1}$, or $\nu L_\nu = 1.5 \times 10^{37} \text{ erg s}^{-1}$. The measured brightness temperature exceeds $10^{7.7} \text{ K}$ and rules out starbursts and supernova remnants (Nagar et al. 2005).

The nucleus was detected by the Two-Micron All Sky Survey (2MASS; Skrutskie et al. 2006). The observed magnitudes $J = 11.2$, $H = 10.5$, $K_s = 10.0$ imply luminosities $\nu L_\nu \approx (4 - 6) \times 10^{42} \text{ erg s}^{-1}$ in these bands.

3.1.1. The nature of the nuclear emission

The combination of being a sub-parsec scale radio source as well as a luminous hard x-ray source points to the source being an AGN. Further evidence comes from the high luminosity. The source is obscured, as made clear from the x-ray spectrum. The infrared luminosity therefore is a better indication of the true bolometric luminosity. This luminosity, a few $\times 10^{42} \text{ erg s}^{-1}$, is higher than is expected from XRBs or nuclear star formation regions.

Dong & De Robertis (2006) perform a bulge-disk decomposition of NGC 3169 and use the 2MASS K-band luminosity of the galaxy to estimate a central black hole mass $\log(M_\bullet/M_\odot) = 8.2$. Héraudeau & Simien (1998) report the central stellar velocity dispersion $\sigma_* = 163 \text{ km s}^{-1}$, which implies $\log(M_\bullet/M_\odot) \approx 7.8$. Assuming $\log(M_\bullet/M_\odot) \sim 8$ for

simplicity, the corresponding $L_{\text{Edd}} \sim 10^{46} \text{ erg s}^{-1}$. The inferred $L_{\text{bol}} \sim 10^{42} \text{ erg s}^{-1}$ then implies $L_{\text{bol}}/L_{\text{Edd}} \approx 10^{-4}$.

3.2. NGC 3184

This is of type Scd, classified as having an H II nucleus by Ho et al. (1997), and is at a distance of 8.7 Mpc (Tully 1988). It was observed with *Chandra* twice, one month apart, for 40 ks and 25 ks. Both observations used the ACIS-S3 chip. The nuclear x-ray emission appears to consist of two components (Fig. 2), a fainter, point-like source in the north and a brighter, more extended source in the south. The total extent of the nuclear emission is about $4''$ ($\sim 170 \text{ pc}$). Both components are soft and have $\text{HR} \sim -0.8$.

Since the northern component has only ~ 30 counts, detailed spectral fitting is not possible. We check for consistency of the data with different models using unbinned data. An absorbed power-law can be fitted to the data, and despite the degeneracy in the parameters, an intrinsic $N_H \gtrsim 6 \times 10^{21} \text{ cm}^{-2}$ is inconsistent at the $3\text{-}\sigma$ level. Fixing N_H at the Galactic value gives a range of acceptable power-laws with $1.2 \leq \Gamma \leq 2.8$ ($3\text{-}\sigma$ limits). An unabsorbed blackbody with temperature $0.28 \text{ keV} \leq kT \leq 0.56 \text{ keV}$ ($3\text{-}\sigma$ limits) is also consistent with the data. The observed broadband luminosity of this component, corrected for Galactic absorption, corresponds to $L_{0.3\text{--}8 \text{ keV}} \sim 2 \times 10^{37} \text{ erg s}^{-1}$. The difference in count rates between the two observations is not statistically significant, so this source does not vary on month timescales.

There are archival *HST* observations in the UV (WFPC2, F300W) and optical (WFPC2, F606W) of this galaxy. The F606W image has the nucleus on the WF4 chip, and clearly shows a central point source. The nucleus is on the PC chip in the F300W image. There is no central point source detected. Both images also show diffuse nuclear emission and a prominent spiral arm in the central $1''$. Other than the nuclear source in the F606W image, there are no obvious counterparts of the x-ray sources in either the UV or the optical. We note here that the coordinates in the *HST* images are mis-aligned with each other and with the x-ray image. The images were therefore aligned by cross-correlating point sources in each individual image with SDSS sources that are classified as stars. The aligned *HST* images match each other to within $0.5''$, and match the *Chandra* image to within $0.7''$. These offsets are comparable to the absolute astrometric accuracy of both *Chandra* and *HST*.

3.2.1. The nature of the nuclear emission

The fact that we see x-ray emission in the soft band but almost none in the hard band argues against the emission being the continuum from the AGN, whether direct or scattered. The source is not seen in the UV image. Both of these points suggest the presence of heavy obscuration. The observed x-rays could instead be soft emission from circumnuclear ionized gas, if the AGN is completely obscured and what is visible is mostly re-processed radiation. This is in fact the case in some heavily obscured Seyfert 2s (e.g. Bianchi et al. 2006; Levenson et al. 2006; Ghosh et al. 2007), where the dominant emission is the soft emission from the Narrow-Line Region. The *Chandra* and *HST* observations, therefore, are inconclusive regarding whether the source is an AGN, but do not rule out that possibility either.

A stronger argument that the source is an AGN derives from infra-red data. This galaxy is part of the *Spitzer* Infrared Nearby Galaxies Survey (SINGS; Kennicutt et al. 2003). Dale et al. (2006) have used the equivalent width of the PAH feature at $6.2\mu\text{m}$ and the fluxes in a mix of high- and low-ionization lines ([S IV] $10.51\mu\text{m}$, [Ne II] $12.81\mu\text{m}$, [Ne III] $15.56\mu\text{m}$, [S III] $18.71\mu\text{m}$, [O IV] $25.89\mu\text{m}$, [S III] $33.48\mu\text{m}$, [S II] $34.82\mu\text{m}$) to create diagnostic diagrams that distinguish between AGN and star-forming galaxies. This nucleus falls into the “transition” region between AGNs and H II regions. This suggests an AGN component to the emission exists that may have been diluted because of the large aperture used ($\sim 20''$) to extract the fluxes. In IRAC images the nuclear source is resolved ($\sim 3.5''$ FWHM compared to the $\sim 1.7''$ FWHM of the PSF). Nuclear fluxes were extracted using $3''$ apertures in the IRAC channels (D. A. Dale, private communication). Host galaxy emission appears to dominate the MIPS (24, 70, and $160\mu\text{m}$) fluxes, but the observed IRAC colors, $[3.6] - [4.5] = -0.26$ and $[5.8] - [8.0] = +0.59$ (magnitudes in AB_ν system), are redder than those of normal late-type galaxies (Assef et al. 2007). This is expected if there is an AGN, as AGN power-law emission falls off more slowly than galactic emission in the NIR. Thus, the IR line ratios and IRAC colors strongly argue for the source to be an AGN.

The nucleus was also detected by 2MASS. The J , H , and K_s magnitudes, from the 2MASS Point Source Catalog (2MASS PSC), are $J = 13.3$, $H = 12.7$, and $K_s = 12.5$, which correspond to $\nu L_\nu \sim 10^{41} \text{ erg s}^{-1}$. Such a luminosity can be easily produced by an AGN. While all the observations are consistent with there being an AGN in NGC 3184, we cannot rule out a nuclear super-starcluster as the source. The x-ray emission could be from one or more XRBs in such a cluster. This possibility is discussed further below.

The x-ray luminosity ($\sim 10^{37} \text{ erg s}^{-1}$) is in the range seen from XRBs. The presence of a nuclear star formation region is indicated by the optical line ratios observed by Ho et al. (1997). In addition, Larsen (2004) reports a candidate nuclear star cluster in NGC 3184.

However, a nuclear star cluster by itself cannot easily explain the multi-wavelength properties observed. The reported value of $E(B - V) = 0.44$ (Ho et al. 1997) corresponds to $1.4 \leq A_V \leq 2.2$ for $3.2 \leq R_V \leq 5$. The observed $m_{\text{F606W}} = 19.2$ corresponds to $m_V = 18.9$ for an O-type stellar spectrum. A distance modulus of 29.7 thus implies $-13 \leq M_V \leq -12.2$. The observed 2MASS K_s -band magnitude, assuming no extinction, implies $M_K = -17.2$, giving $4.2 \leq (V - K)_0 \leq 5.0$. A young star cluster would have a bluer color. An old cluster is ruled out by the presence of hydrogen emission lines which require the presence of the ionizing continuum produced by O and B stars. We compare the observed properties with those of a star cluster simulated with Starburst99 (Leitherer et al. 1999; Vázquez & Leitherer 2005). The comparison is qualitative, as the values of the input parameters, for example the total mass, the age, and the metallicity of the cluster, are all unknown. We therefore use the default parameter values in Starburst99, namely $M_{\text{tot}} = 10^6 M_\odot$, metallicity $Z = 0.02$, and instantaneous star formation with a Kroupa IMF ($\alpha = 2.3$ for $100 \leq M/M_\odot \leq 0.5$, $\alpha = 1.3$ for $0.5 \leq M/M_\odot \leq 0.1$). We choose to match the absolute magnitude in the K band, where extinction is likely to be small. The simulated cluster never reaches $M_K = -17.2$. We instead consider the K -magnitude at ages less than the lifetime of O stars. At ~ 3 Myr, $M_K \sim -15.5$. The difference $\Delta M = 1.7$, or a factor of ~ 5 in flux, can be accounted for by scaling up the mass of the cluster to $5 \times 10^6 M_\odot$. We assume that this ΔM applies to all bands. Then $M_V = -16.8$, and the extinction required is $A_V = 6$ mag, which is not unreasonable towards the center of spiral galaxy. This amount of extinction would also explain the non-detection of the cluster in the F300W image. The upper limit $m_{\text{F300W}} > 19.0$ corresponds to $m_U > 18.3$. Assuming a standard interstellar extinction law, $A_U \sim 1.5 A_V = 9$ mag. The corrected absolute magnitude of the simulated cluster is $M_U = -18.1$. The expected apparent magnitude is $m_U = 20.6$, consistent with the limit. However, in this case $E(B - V) \sim 1.2 - 1.9$ is discrepant with $E(B - V) = 0.44$ obtained via the Balmer decrement. The high extinction also increases the inferred x-ray luminosity, to $L(0.3 - 8\text{keV}) \approx 1 \times 10^{38}$ erg s $^{-1}$ for a power-law model with $\Gamma = 2$, or $L(0.3 - 8\text{keV}) \approx 8 \times 10^{38}$ erg s $^{-1}$ for thermal Bremsstrahlung with $kT = 0.3$ keV. The former value is still consistent with an XRB source, and in fact the source lies in the LMXB region in the color-color diagram of Prestwich et al. (2003). A cluster with O and B stars, however, is too young to have formed LMXBs. Any XRB that exists should be an HMXB.

In conclusion, there are two scenarios that are consistent with the observations. In both there is a nuclear star cluster that dominates the optical emission. In the first, there is no AGN and the x-rays are produced by one or more XRBs. As the simulation shows, a “typical” cluster does not reproduce the observed properties. But because the age, stellar and gas masses, dust-to-gas ratio, metallicity, star formation rate, and IMF are all unknown, the parameter space available is large, and we do not rule out the possibility that some physically

plausible combination of parameters exists that could explain all the observations. In the second, there is a low-luminosity AGN in the center of the star cluster, so heavily obscured that we do not observe any direct or scattered emission. The x-ray emission arises from photoionized gas immediately surrounding the AGN. Using the luminosity derived using the Bremsstrahlung model above, and assuming that approximately 1% of the AGN luminosity is reprocessed into the plasma x-ray emission, the AGN has a luminosity $\sim 10^{41}$ erg s $^{-1}$. The infrared line ratios and IRAC colors from *Spitzer* strongly argue for this scenario.

3.3. NGC 4102

This is an Sb galaxy, classified as H II in Ho et al. (1997) and as H II/LINER in the NASA/IPAC Extragalactic Database (NED), at a distance of 17 Mpc (Tully 1988). The *Chandra* observation of this galaxy was presented in Dudik et al. (2005). There are about 350 counts in the x-ray image of the nucleus. As a hardness ratio map (Fig. 3) shows, the hard and soft emission are well segregated into a fairly hard ($HR = -0.20 \pm 0.08$), point-like source with extended, very soft ($HR = -0.88^{+0.03}_{-0.06}$) emission to the west of it. *Wavdetect*, run on hard and soft band images, detects a small hard source and an encompassing soft source whose centers are 1'' apart. We therefore fit the spectra of the harder “core” and the softer extended emission separately, using counts from the regions shown in Fig. 3. The spectrum of the core has 171 counts, and shows a broad line between 6 and 7 keV, suggestive of reflection. The spectrum was fit after binning to 5 counts per bin, using the Cash statistic (*cstat* in *Sherpa*). A simple absorbed power-law model, fit to the energy range 0.3–3 keV, shows increasingly positive residuals at energies above 3 keV, again suggestive of a reflection component. The fit quality is poor, with a statistic value of 200 for 27 d-o-f. Using a reflection model (*xspexrav*) reduces the statistic to 60 for 26 d-o-f. The possible line at 6.4 keV is not well constrained because of the lack of counts on the high energy side of the line (there are 8 counts with $E > 7$ keV). For the line, we added a Gaussian at the fixed position of 6.4 keV and of fixed FWHM 0.3 keV, allowing only the amplitude to vary. This reduces the statistic further, to 40 for 25 d-o-f. The final parameters are $\Gamma = 2.2^{+0.6}_{-0.5}$ and reflection scaling factor $R = 129^{+283}_{-85}$. Though the uncertainty is large, the high value of R indicates that the reflected component dominates over the direct emission in the observed radiation. The formal equivalent width of the line is 2.5 keV, but the uncertainty in the amplitude of the line is of the order of $\sim 50\%$ and in the normalization of the reflected component, $\sim 30\%$. The flux, excluding the line and corrected for Galactic absorption, is $F(0.3-8 \text{ keV}) = 4.2 \times 10^{-13}$ erg cm $^{-2}$ s $^{-1}$. A fit using the χ^2 statistic (shown in 4) gives best-fit parameter values consistent with those from the Cash fit, with the exception of the equivalent width of the line, which is 3.3 keV in this fit. Given the poor determination of the

continuum near the line the difference is not significant. The fact that the best-fit equivalent width values are large is another indication that the direct emission is not being detected.

The extended emission is very soft, with just 5 counts (out of 115) above 2.5 keV. The spectrum was fit after binning to 5 counts per bin and using both the χ^2 and Cash statistics. A bremsstrahlung model provides an acceptable fit ($\chi^2 = 9.6$ and Cash statistic = 30 for 18 d-o-f), and the MEKAL model is less favored ($\chi^2 = 15.6$ and Cash statistic = 41 for 18 d-o-f). Best-fit parameter values obtained using the two statistics are consistent within the errors. The best-fit temperature $kT \sim 1$ keV is higher than what may be expected of 100 pc-scale circumnuclear gas. The plasma surrounding an AGN may be photoionized rather than collisionally ionized, and there may be complexity in the spectrum that is hidden because of the poor quality. The orientation of the extended x-ray emission coincides with an outflow seen in [O III] emission (Ganda et al. 2006). The flux in the extended emission is $F(0.3-8 \text{ keV}) \approx 2 \times 10^{-13} \text{ erg cm}^{-2} \text{ s}^{-1}$. Spectral models and best-fit parameter values for both the core and the extended emission are shown in Table 4. The χ^2 fits for both the core and extended components are shown in Fig. 4.

The nucleus was detected by 2MASS. The 2MASS PSC gives $J = 10.9$, $H = 9.8$, and $K_s = 9.2$. For a distance of 17 Mpc, these correspond to $\nu L_\nu(J) \approx 6 \times 10^{42} \text{ erg s}^{-1}$, $\nu L_\nu(H) \approx 8 \times 10^{42} \text{ erg s}^{-1}$, and $\nu L_\nu(K_s) \approx 7 \times 10^{42} \text{ erg s}^{-1}$. The luminosity would be a factor of ~ 2 lower for the distance ~ 11 Mpc used by Dudik et al. (2005). The nucleus was also detected in radio by the FIRST survey (1.4 GHz). The stated radio position is within $0.5''$ of the *Chandra* position, and therefore within *Chandra* astrometric accuracy. The radio beam size, however, was $3.75'' \times 2.84''$. The integrated radio flux density was 223 mJy, with peak flux density of 167 mJy.

3.3.1. The nature of the nuclear emission

Individually, the x-ray, IR, and radio observations have enough uncertainty that it is not possible to identify the source as an AGN. However, the fact that the x-ray source has a hard spectrum with a line at roughly 6.4 keV, that the nucleus is a radio source, and that the luminosities implied in the IR are as high as $\sim (7-8) \times 10^{42} \text{ erg s}^{-1}$, together make it unlikely that the source is not an AGN. The x-ray spectrum in fact suggests that the source is a heavily obscured AGN. The high value of the reported color excess $E(B-V) = 1.0$ (Ho et al. 1997) also supports this hypothesis.

Ganda et al. (2006) report $\sigma_* = 150 \pm 10 \text{ km s}^{-1}$, which implies $\log(M_\bullet/M_\odot) = 7-8$. If we assume the infrared luminosity is representative of the bolometric luminosity of the

AGN, then $L/L_{\text{Edd}} \sim 10^{-3} - 10^{-4}$.

3.4. NGC 4647

NGC 4647 is a galaxy of type Sc, its nucleus classified as H II in Ho et al. (1997), at a distance of 16.8 Mpc (Tully 1988). The *Chandra* observation is of the elliptical galaxy NGC 4649, and NGC 4647 is on the chip, at an off-axis angle of $\sim 2.5'$. Two factors complicate the detection of the nucleus of NGC 4647. First, the nucleus lies within the extended emission from NGC 4649. Second, the nucleus falls on a node boundary of the CCD. *Wavdetect* at its default filter for source significance (~ 1 false source per 10^6 pixels) does not detect the nucleus. However, once the elliptical galaxy is modeled and subtracted out of the image, there is a positive residual at the location of the nucleus of NGC 4647 (see Fig. 5). To extract source counts we used a circular region centered on the centroid of the residual and with radius $2.3''$, which is approximately the 95% encircled-energy radius at 1.5 keV at that position. To extract background counts we located another region on the same node boundary that was at the same distance from the center of NGC 4649 as was the source circle. The source region has ~ 11 counts after background subtraction, but this number necessarily has a large uncertainty. We take the radius of the source circle, $2.3''$, as the *Chandra* positional uncertainty of this source.

The nucleus may also have been detected in x-rays by XMM-Newton (Randall et al. 2006). While the source was detected with $S/N = 11$, the positional uncertainty was $3''$. The XMM-Newton source is soft, similar to the *Chandra* residual. The XMM-Newton and *Chandra* source positions differ by $5.2''$. There is a nuclear 2MASS point source ($K_s \approx 12.3$) at a distance of $1.1''$ from the *Chandra* position, but it is embedded in diffuse emission and the flux from the point source is poorly constrained. In the radio, there is a 5σ upper limit to the nuclear emission of 0.5 mJy at 5 GHz (Ulvestad & Ho 2002). There is an older report of a radio detection of the nucleus with a flux density of 16 mJy at 1.4 GHz (Willis et al. 1976; Kotanyi 1980), but with positional uncertainty $(\Delta\alpha, \Delta\delta) = (0.16s, 11.2'')$.

3.4.1. The nature of the nuclear emission

The data are inconclusive at this time as to whether there is an AGN in NGC 4647. The faintness of the source and the positional uncertainties in the existing observations prevent a firm identification and characterization of the source.

3.5. NGC 4713

This galaxy is of type Sd, at a distance of 17.9 Mpc (Tully 1988). Its nucleus was classified as T2 (transition object with type 2 spectrum) by Ho et al. (1997). The nucleus is clearly detected by *Chandra*, but with only ten counts. It is a very soft source, with nine of the ten counts below 2.5 keV. This object was also analyzed by Dudik et al. (2005), but since they were looking for hard-band sources, this object was not counted as a detection. The observed count rate corresponds to a flux of $(5\text{--}10)\times 10^{-14}$ erg cm $^{-2}$ s $^{-1}$ in the 0.3–8 keV band, or luminosity $(3\text{--}5)\times 10^{38}$ erg s $^{-1}$ for our assumed distance. The 2–10 keV flux depends strongly on the assumed model, from $f_X \sim 1 \times 10^{-17}$ erg cm $^{-2}$ s $^{-1}$ for a thermal bremsstrahlung model with $kT = 0.3$ keV, to $f_X \sim 5 \times 10^{-15}$ erg cm $^{-2}$ s $^{-1}$ for a power-law with $\Gamma = 2$ and Galactic absorption.

NGC 4713 was observed by *HST* in December 2006 (Martini et al. 2008, in prep.). The nucleus is resolved; thus only a nuclear star cluster or star forming region, and no AGN, is detected. The cluster is $\sim 0.40''$ in diameter in the image, corresponding to a physical size of ~ 35 pc. Within this aperture the flux density is $f_\lambda = 5.34 \times 10^{-17}$ erg cm $^{-2}$ s $^{-1}$ Å $^{-1}$, which implies $\nu L_\nu = 1.2 \times 10^{40}$ erg s $^{-1}$. The nucleus is also in the 2MASS PSC, with J , H , K_s luminosities $\nu L_\nu \sim 10^{41}$ erg s $^{-1}$. However, the nucleus is embedded in diffuse extended emission and therefore the reported magnitudes may not be accurate estimates of the nuclear emission. There is an upper limit of 1.1 mJy to the nuclear radio emission at 15 GHz (Nagar et al. 2005), and a similar limit, 1.0 mJy, to the emission at 1.4 GHz from the FIRST survey.

3.5.1. The nature of the nuclear emission

As in the case of NGC 4647, the data are inconclusive regarding the presence of an AGN. The data are consistent with the AGN hypothesis: the “transition object” classification by Ho et al. (1997) implies there may be an AGN component in the optical spectrum; the nucleus is without doubt an x-ray source, though it is not possible to distinguish between emission from circumnuclear gas and the nucleus proper in the current *Chandra* imaging. The hardness ratio (with large uncertainty) is consistent with a $\Gamma = 2$ power-law. NGC 4713 may be similar to NGC 3184 in having a low-luminosity AGN inside a nuclear star cluster.

3.6. NGC 5457 (M 101)

NGC 5457 is a galaxy of type Scd at a distance of approximately 7 Mpc (Freedman et al. 2001; Stetson et al. 1998). The nucleus was classified as H II by Ho et al. (1997). It has been observed multiple times by *Chandra* for a total observation time of about 1.1 Ms. Our analysis omits the shorter, and hence low signal-to-noise, exposures. The observations included here are listed in Table 3. The total usable exposure time is 695 ks. *Chandra* clearly resolves two sources in the nuclear region (Fig. 6), which we label N and S. The northern source, N, is the nucleus, while the southern, S, is a star cluster (Pence et al. 2001). Table 3 shows the counts and hardness ratios of the two sources in each of the observations. Source N (the nucleus) varies in brightness by about a factor of 9 over the course of about 8 months (see Table 3 and Fig. 7). There is no significant change in hardness ratio. In our analysis and discussion below we consider only the nucleus (source N).

Three nuclear x-ray spectra were extracted: one (“merged”) from the event list obtained by merging all observations done in 2004, and fit using the instrument response from ObsID 5339; one (“high state”) from merging two observations where the source had a high count rate (ObsIDs 4736 and 6152) and fit using the response from ObsID 4736; and one (“low state”) from merging five observations where the count rate was low (ObsIDs 5300, 5309, 4732, 5322, 5323), fit using the response from ObsID 4732. The spectra are shown in Figs. 8 and 9; fit models and parameters are shown in Table 4. The low state spectrum can be fit with an absorbed power-law ($\chi^2/\text{dof} = 18.7/30$) but the fit is improved slightly with the addition of a plasma component (*xsmekal*) at temperature $kT = 0.3$ keV ($\Delta\chi^2 = -4.5$ for two fewer d-o-f). The best-fit power-law slope $\Gamma = 1.7 \pm 0.5$ is typical of unabsorbed AGN, and best-fit intrinsic absorption is consistent with zero. The unabsorbed 0.3–8 keV luminosity is $\sim 3 \times 10^{37}$ erg s $^{-1}$. The high state spectrum can also be fit by an absorbed power-law. The best-fit slope is $\Gamma = 2.2^{+0.4}_{-0.3}$, steeper but consistent with the low state slope within the uncertainties. The differences from the low state spectrum are, first, that the fit requires intrinsic absorption ($N_H \sim 10^{21}$ cm $^{-2}$), and second, that there is no evidence for the MEKAL component. If a plasma component exists in the high state its flux falls below that of the power-law component. The unabsorbed 0.3–8 keV luminosity in the high state is $\sim 3 \times 10^{38}$ erg s $^{-1}$. Figure 10 shows the high and low state spectra over-plotted. The spectra are identical below 1 keV, with the entire flux difference arising from the power-law normalization between 1 and 7 keV, and a possible “shoulder” between 1 and 2 keV in the high state. A fit where the power-law slope is forced to be identical in the low and high states is of similar statistical significance and produces best-fit values similar to the separate fits. This fit is shown in Table 4 in the rows labeled “sim. low” and “sim. high”. The merged spectrum is similar to the high state one in that an absorbed power-law provides a good fit without the need for additional components.

We analyzed archival *HST* WFPC2 images of M101, a 2400 s exposure using the F336W filter (referred to as U band below; nucleus on WF3) and a 1600 s exposure using the F547M filter (referred to as V band below; nucleus on PC1). The nucleus and the star cluster are detected in both images. In 2-pixel radius apertures, the U band nuclear flux is 6.3×10^{-17} erg cm $^{-2}$ s $^{-1}$ Å $^{-1}$ and the V band flux is 8.3×10^{-17} erg cm $^{-2}$ s $^{-1}$ Å $^{-1}$, corresponding to $m_{\text{F336W}} = 19.3$ and $m_{\text{F547M}} = 19.0$ in the STMAG system. The 2MASS PSC contains a source at the position of the nucleus (x-ray source N) but none at the location of source S. The given magnitudes $J = 13.1$, $H = 12.5$, and $K_s = 11.8$ all correspond to $\nu L_\nu \approx 10^{41}$ erg s $^{-1}$. The nucleus was not detected by FIRST. Heckman (1980) gives an upper limit to the nuclear luminosity at 6 cm corresponding to $\nu L_\nu < 6 \times 10^{35}$ erg s $^{-1}$.

McElroy (1995) reports $\sigma_* \approx 78$ km s $^{-1}$ which implies $\log(M_\bullet/M_\odot) \approx 2 \times 10^6$. The corresponding Eddington luminosity is $L_{\text{Edd}} \approx 3 \times 10^{44}$ erg s $^{-1}$. Assuming the source is an AGN, and assuming bolometric correction factors of ~ 10 and ~ 1 in the x-ray and IR, respectively, implies that the bolometric luminosity is in the range 10^{39} – 10^{41} erg s $^{-1}$, or that $L/L_{\text{Edd}} \sim 10^{-5}$ – 10^{-3} .

3.6.1. The nature of the nuclear emission

The case for the nuclear source being an AGN rests on the following. *Luminosity*: The IR luminosity, $\sim 10^{41}$ erg s $^{-1}$, seen by 2MASS, would require either a super-starcluster or an improbably high number ($\gtrsim 10^3$) of x-ray binaries. The plausibility of a super-starcluster is examined below. *Variability*: The source varies by a factor of nine in eight months in 2004, and also varied between 2000 and 2004. *X-ray spectrum*: The spectrum is an absorbed power-law with slope ~ 2 . In particular, the spectrum cannot be fit by a thermal component alone — a power-law is necessary. The low state spectrum is reminiscent of highly obscured AGN where an unabsorbed but diminished spectrum is seen via scattering. *X-ray colors*: the ratio of 0.3–2 keV, 2–5 keV, and 5–8 keV counts puts this object into the Compton-thick AGN part of the Levenson color-color diagram (Fig. 9 in Levenson et al. 2006).

The x-ray properties of the nucleus are consistent with both the XRB and AGN hypotheses, but an AGN is not ruled out. The inferred x-ray luminosity (10^{37} – 10^{38} erg s $^{-1}$) is in the range seen from XRBs, and the observed x-ray colors put this source in the LMXB region of the Prestwich et al. (2003) color-color diagram. But here too, the H II region requires a cluster with O and B stars, and consequently the cluster could contain HMXBs but would be too young to have formed LMXBs. In favor of the XRB scenario is that the variability of the source is similar to the spectral state changes in XRBs. The low state may be interpreted as being the XRB state known as “hard” or “low/hard”, and the best-fit power law slope,

$\Gamma \sim 1.7$ is the value seen in XRBs in this state. The high state would then be the XRB state known as the “very high” or “steep power law” state. The best-fit power-law slope $\Gamma \sim 2.2$ in this case is less steep than is usually seen in XRBs in this state ($\Gamma \gtrsim 2.4$) but the steeper value is included in the 90% confidence range. However, it must be kept in mind first, that at the quality of the spectra analyzed here the power law slopes are consistent with being identical in the two states, and second, that AGNs show the same state behavior (e.g. 1H 0419-577, Pounds et al. 2004).

A comparison of the super starcluster scenario with the observations proceeds very similarly to the one made in the case of NGC 3184. The distance modulus for M 101 is 29.3, and the 2MASS observation thus implies $M_K = -17.5$ assuming no extinction. For our simulated cluster this requires a mass of $6 \times 10^6 M_\odot$. The *HST* magnitudes converted to the Vega system are $m_V = 19.0$ and $m_U = 19.6$. Therefore $M_V = -10.3 - A_V$. To estimate the extinction we use $E(B - V) = 0.33$ (Ho et al. 1997) and assume $3.2 \leq R_V \leq 5$. This gives $1.1 \leq A_V \leq 1.7$, and thus $-12.0 \leq M_V \leq -11.4$. This implies that $5.5 \leq (V - K)_0 \leq 6.1$, much redder than a young star cluster. Conversely, the simulated cluster has $M_V = -17.1$, and so the measured apparent magnitude requires $A_V = 6.8$, which in turn implies $1.4 \leq E(B - V) \leq 2.1$ for the range of R_V mentioned above. This is inconsistent with the value derived by Ho et al. (1997), and the implied hydrogen column density $N_H \sim 10^{22} \text{ cm}^{-2}$ is an order of magnitude higher than that obtained from the x-ray spectrum in the high state. The caveat here, as mentioned in the section on NGC 3184, is that the large number of free parameters in the cluster simulation makes the above comparison only qualitative. A comparison with a real star forming region, the Orion Nebula, also shows this discrepancy in reddening. The observed source color is $(m_{\text{ST,F336W}} - m_{\text{ST,F547M}}) = +0.30$. The unreddened color predicted by the *HST* IRAF tool Synphot is -1.90 . This implies $E(B - V) = 1.12$ using the Cardelli, Clayton, & Mathis (1989) reddening law or $E(B - V) = 0.99$ using the Howarth (1983) LMC reddening law in Synphot. This implies $N_H = 6 \times 10^{21} \text{ cm}^{-2}$ assuming Galactic gas-to-dust ratio or $\sim 10^{22} \text{ cm}^{-2}$ for LMC gas-to-dust ratio.

Thus, there are again two possible scenarios, as in the case of NGC 3184. The x-ray source could be an HMXB in a super-star cluster. The star cluster would dominate the optical and IR emission. The large variation observed in the x-ray flux rules out the source’s being more than one HMXB, as otherwise they would have to be varying in concert. As the above discussion shows, in this scenario accounting for the extinction is not straightforward. The actual amount of obscuration is important, however, for the plausibility of the HMXB hypothesis since the inferred x-ray luminosity ($\sim 10^{38} \text{ erg s}^{-1}$ in the high state) is already at the high end of the range of XRB luminosities and there is not much room for a significantly higher absorption-corrected intrinsic luminosity. The alternative scenario is an AGN together with a nuclear star cluster. In AGNs both the intrinsic luminosity and the amount of

obscuration are known to vary. The low state x-ray spectrum may be explained as a truly under-luminous (10^{37} erg s $^{-1}$) unabsorbed AGN, or as an AGN where the obscuration is so high that only scattered light, and no direct emission, is seen. The fact that the x-ray colors are similar to those of Compton-thick AGN (Levenson et al. 2006) supports the latter view, but we also note the absence of the 6.4 keV Fe K α line in the x-ray spectrum that is often present in the reflected component. Finally, the issue of extinction and reddening is readily explained if there is an AGN, as an AGN has additional sources of obscuration (the “torus”) that affect its radiation but not that of the cluster. Without knowledge of the fractional contribution of the AGN and the cluster to the observed fluxes in the different bands, it is impossible to accurately estimate the reddening from the colors. Though both the HMXB and AGN hypotheses are possible, on balance the AGN appears to be the more plausible one.

4. Discussion

The motivation for this paper was to evaluate the feasibility of detecting low-mass SMBHs in late-type spiral galaxies, which should be accreting at the current epoch and so should be detectable in x-rays. The six galaxies studied in this paper are not all late-type, but span the range Sa–Sd. NGC 3169 and NGC 4102 were regarded as low luminosity AGNs. None of the remaining four nuclei, however, was known to have an accreting SMBH, of any mass. NGC 3169 and NGC 4102 are of type Sa and Sb, which have massive bulges and are expected to have massive SMBHs. For galaxies of types Scd and Sd, on the other hand, the lack of a luminous AGN could mean either that there is no SMBH or that the mass of the SMBH is low. As such, the observations studied here examine both aspects of a search for accreting low-mass SMBH: First, are these objects really detectable, given that the accretion rate is expected to be low? Second, are any sources detected in the very latest type spiral galaxies that have small or no bulges?

We first note that of the six galaxies presented here, all six show nuclear x-ray sources. This implies that it is a very common occurrence. In a survey of late-type spiral galaxies such as our ongoing *Chandra* survey, therefore, the predominant concern is not going to be detection efficiency, but rather identification of the AGNs among the detected sources. Given that the sample presented in this paper consists of only six galaxies, we do not draw quantitative conclusions here of the prevalence of very low-luminosity AGNs in nearby galaxies. But we note that, as shown in §§3.1–3.6, of the six nuclear x-ray sources, two, NGC 3169 and NGC 4102, are almost certainly AGNs, two, NGC 3184 and M 101, have very strong, though not conclusive, arguments in favor of their being AGNs. The two remaining

galaxies, NGC 4713 and NGC 4647, are ambiguous but AGNs are not ruled out. We discuss below the issues such surveys will face when attempting to identify the nature of the detected sources. The diagnostic tools currently used to distinguish AGN from non-AGN were developed in the course of studying luminous AGN. Dilution of the AGN emission by host galaxy light was not a serious problem and observations with low spatial resolution (several arcseconds) sufficed. In the study of AGN that are either intrinsically less luminous or are heavily obscured, however, host galaxy light becomes increasingly problematic, to the point where signs of AGN emission are barely, or not at all, detected by the usual diagnostics. This problem will persist until observations with angular resolution of 1–10 mas become possible so that host galaxy light can be effectively excluded, though it can be mitigated by using regions of the spectrum where host galaxy emission is negligible, for example very high energy x-rays (tens to hundreds of keV) or radio (if the AGN happens to be radio loud).

Other sources of radiation in the vicinity of the AGN are, for example, plasma photoionized by the AGN itself, or a nuclear star cluster. The targeted AGNs have very low luminosity and thus even moderate amounts of obscuration may cause a significant decrement in the observed flux. In most cases, therefore, the AGN contribution should not be expected to dominate the total observed flux. Consequently, identifying these AGNs requires a different approach than what can be used in the case of the more luminous AGNs (Seyferts and QSOs). AGNs can be identified using x-ray observations (e.g. with *Chandra* and *XMM-Newton*) solely, but only if they are point sources whose inferred luminosities are greater than $\sim 10^{41}$ erg s $^{-1}$. Below that value, AGNs can become indistinguishable from ULXs and XRBs in x-rays. ULXs can have luminosities of a few times 10^{40} erg s $^{-1}$ (e.g. Soria et al. 2007) and have x-ray spectra that look similar to AGN spectra. It has been suggested (Stobbart et al. 2006) that ULX spectra show a break at ~ 5 keV. AGNs are not known to show this break. In high quality spectra with a large number of counts it may be possible to exploit this difference to separate ULXs and AGNs. XRBs have power law spectra with $\Gamma \sim 2$, can show an Fe K α emission line, and emit hard x-rays, all characteristics of AGNs as well. Additionally, even with *Chandra*'s angular resolution, the physical space probed ranges from the central $\sim 10 - 100$ pc of the galaxy. The existence of one or more XRBs within that region would be unsurprising. However, the fact that the inferred luminosities are as high as 10^{38} erg s $^{-1}$ severely constrains the expected number of XRBs. For example, for M 101, one of the four galaxies presented here that are not confirmed AGNs, Pence et al. (2001) provide a log N-log S relation as well as the surface density of x-ray point sources as a function of radius (their Figs. 3 and 4). Approximately 12.5% of the sources have luminosities exceeding 10^{37} erg s $^{-1}$. The surface density of sources in the innermost $0.5'$ is ~ 4.75 arcmin $^{-2}$. Therefore we may expect 0.6 sources arcmin $^{-2}$ above the luminosity cut-off in the central $0.5'$, or $\sim 4 \times 10^{-3}$ such sources within the *Chandra* source circle of radius $2.3''$ that has been used here. M 101

is of type Scd, and can be taken to be representative of the other three galaxies, NGC 4647, NGC 3184, and NGC 4713 which are types Sc, Scd, and Sd, respectively. Thus invoking XRBs and ULXs alone to explain the x-ray observations leads to physically implausible conditions, such as requiring that most, or all, quiescent, non-starburst spiral galaxies have a ULX or ~ 100 XRBs in the central $0.5'' - 2''$. Nevertheless, x-ray observations by themselves will usually be inadequate to distinguish AGNs from non-AGNs in any particular instance.

Information from other wavebands is thus crucial for the identification process. For the six galaxies in this paper multi-wavelength photometry is summarized in Tables 5 and 6. But here too, traditional methods of identifying AGNs using flux ratios such as α_{OX} , α_{KX} , and f_X/f_R , must be used with caution. The low luminosities of the AGNs mean that the emission in the two bands being compared may not be from the same object. For instance, for an obscured AGN surrounded by a nuclear star cluster, the observed x-ray flux may be from the AGN but the optical flux may be dominated by the cluster. The existence of an AGN must instead be inferred by consistency and plausibility checks considering as much of the spectral energy distribution as possible, and the goal is the rejection of the hypothesis that all of the observed properties can be explained without requiring the presence of an AGN. NGC 3184 provides a good example where different modes of observing, imaging and spectroscopy, in two wavebands, x-ray and IR, together make a compelling argument for the presence of an AGN where each observation individually is ambiguous.

Nuclear star clusters are fairly common in spiral galaxies (e.g. Böker et al. 2002; Walcher et al. 2005). Besides making the presence of XRBs more likely, such a cluster can mask the AGN emission. A young cluster with many O and B stars may dominate in the UV in addition to the optical, but the emission would fall rapidly towards redder wavelengths, whereas an AGN power law emission does not. Thus adding an AGN component to the spectrum of a young cluster makes the overall spectrum redder than expected from a cluster. This appears to be the case in NGC 3184 and NGC 5457.

In addition to the spectral energy distribution, source variability can be a discriminant, as AGNs are known to vary in all wavelengths, whereas a star cluster, say, would not. Conversely, if the variation is periodic it would rule out an AGN and argue for an XRB instead.

A survey of the type discussed here finds AGNs and strong AGN candidates, but does not measure the masses of the SMBHs in those AGNs. Measurement of the mass of one of these SMBHs will be a difficult endeavor, since the sphere of influence of the black hole cannot be resolved with current technology and resources. None of the six objects studied in this paper shows broad optical emission lines whose widths could be used to estimate the BH mass, and this is likely to be typical behavior. Spectropolarimetry may uncover broad lines

in polarized light in some of the AGNs. Estimates of the SMBH mass may be made by using known scaling relationships, with the caveat that the correlations are all based on SMBHs two or more orders of magnitude more massive than the ones expected to be found by the survey. The least indirect method is an application of the observed correlation between the x-ray power law slope and Eddington ratio (Williams et al. 2004). The Eddington ratio and the luminosity in turn provide an estimate of the mass of the SMBH. Other relationships that can be used are: (a) the M_{\bullet} – σ relation (Ferrarese & Merritt 2000; Gebhardt et al. 2000), but this method becomes more and more uncertain as the bulge itself becomes ill-defined in the latest-type spirals; (b) the M_{\bullet} – L_{bulge} relationship (Kormendy & Richstone 1995; McLure & Dunlop 2001; Marconi & Hunt 2003), which has more scatter and also faces the problem of the definition of the bulge; (c) the M_{\bullet} – v_{circ} relation (Ferrarese 2002; Baes et al. 2003), which has the advantage that it does not require the presence of a well-defined bulge; (d) the M_{\bullet} – C relation (Graham et al. 2001), where C is the concentration of light. There is also a reported relationship between black hole mass and core radio power (Snellen et al. 2003; McLure et al. 2004), but this relationship is not as well established as the others, and is based on observations of elliptical galaxies, so its applicability to the spiral galaxies here is uncertain. Overall, there is unlikely to be one standard method of measurement that can be applied to these galaxies, but one or more of the above methods may provide useful estimates of or limits to the masses of the SMBHs in these AGNs. Mass measurements independent of the scaling relationships are possible if an object turns out to have broad emission lines, like NGC 4395, in which case line widths or reverberation mapping may be used, or if it has maser emission, like NGC 4258, in which case gas dynamics can be used. Mass measurement in other cases will have to await mas-scale angular resolution in bands other than radio to resolve the sphere of influence of these black holes.

Of the six galaxies here, NGC 3169, NGC 4102, and M 101 have measurements of either the stellar velocity dispersion or the luminosity of the bulge, thus allowing an estimate of their SMBH masses (assuming here that the source in M 101 is an AGN). The scatter in the M_{\bullet} – σ and M_{\bullet} – L_{bulge} relations, together with the uncertainty in the observed flux and the bolometric correction, result in uncertainties of about an order of magnitude in the inferred Eddington ratio, but all three objects have $L/L_{\text{Edd}} \sim 10^{-4}$. This is in the range seen in low-luminosity AGNs (e.g. $L \sim 10^{-5}L_{\text{Edd}}$ for M 81; Young et al. 2007), and much higher than the $L \sim 10^{-9}L_{\text{Edd}}$ seen in truly quiescent SMBHs. These observations indicate that there is indeed a population of accreting SMBHs in nearby spiral galaxies that do not show optical signs of activity but can be uncovered by looking for their x-ray emission. Such a population will answer the question of whether the bulge is the dominant component that determines the existence, and mass, of a nuclear SMBH. The known AGN in the Sd galaxy NGC 4395, and the strong evidence for AGNs in the Scd galaxies NGC 3184 and NGC 5457

suggest it is not, at least as far as existence is concerned. Among the SMBHs discovered in the latest-type spirals (with small or no bulges) and in the lowest-mass galaxies should be a population of SMBHs with masses less than $10^6 M_\odot$, providing, for the first time, a way to investigate the low-mass end of the local supermassive black hole mass function.

We thank D. A. Dale for kindly providing *Spitzer* fluxes for the nucleus of NGC 3184, and P. Martini, T. Boeker, and E. Schinnerer for providing *HST* data for NGC 4713 prior to publication. This research has made use of the NASA/IPAC Extragalactic Database (NED) which is operated by the Jet Propulsion Laboratory, California Institute of Technology, under contract with the National Aeronautics and Space Administration. This publication makes use of data products from the Two Micron All Sky Survey, which is a joint project of the University of Massachusetts and the Infrared Processing and Analysis Center/California Institute of Technology, funded by the National Aeronautics and Space Administration and the National Science Foundation.

Facilities: CXO (ACIS), HST (WFPC2,ACS), Spitzer (IRAC,MIPS)

REFERENCES

- Assef, R. J. et al. 2007, ApJ, in press, (ArXiv e-prints 0708.1513)
- Baes, M., Buyle, P., Hau, G. K. T., & Dejonghe, H. 2003, MNRAS, 341, L44
- Barth, A. J., Ho, L. C., Rutledge, R. E., & Sargent, W. L. W. 2004, ApJ, 607, 90
- Bianchi, S., Guainazzi, M., & Chiaberge, M. 2006, A&A, 448, 499
- Böker, T., Laine, S., van der Marel, R. P., Sarzi, M., Rix, H.-W., Ho, L. C., & Shields, J. C. 2002, AJ, 123, 1389
- Cardelli, J. A., Clayton, G. C., & Mathis, J. S. 1989, ApJ, 345, 245
- Dale, D. A. et al. 2006, ApJ, 646, 161
- de Vaucouleurs, G., de Vaucouleurs, A., Corwin, Jr., H. G., Buta, R. J., Paturel, G., & Fouque, P. 1991, Third Reference Catalogue of Bright Galaxies (Volume 1-3, XII, 2069 pp. 7 figs. Springer-Verlag Berlin Heidelberg New York)
- Dolphin, A. E. 2002, in The 2002 HST Calibration Workshop : Hubble after the Installation of the ACS and the NICMOS Cooling System, Proceedings of a Workshop held at the

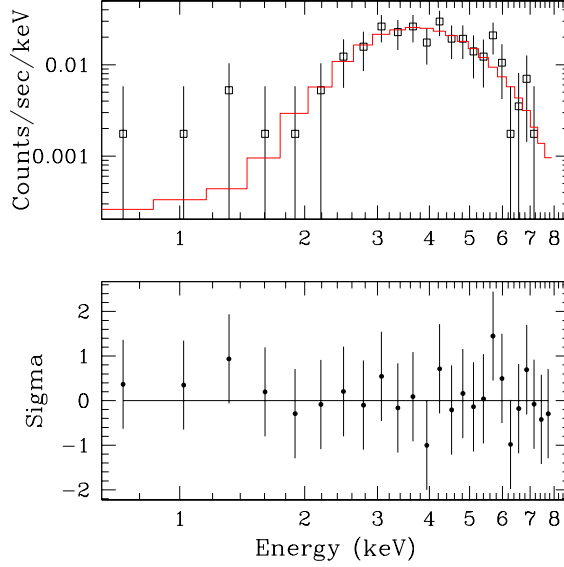


Fig. 1.— Spectrum of NGC 3169. Squares show the data binned by 20 PHA channels. The solid line shows the best-fit model, an absorbed power-law with $N_H \sim 10^{23} \text{ cm}^{-2}$, and $\Gamma = 2.6$. The lower panel shows the residuals from the fit.

Table 1. Targets and observation parameters

Target	Type	Nucleus ^a	Coordinates (J2000)		Dist. ^b	Scale	Obs. Date	ObsID	Exp.
			RA	Dec	(Mpc)	(pc/'')			(ks)
NGC 3169	Sa	LINER	10 14 15.0	+03 27 58	19.7	96	2001 May 2	1614	2.0
NGC 3184	Scd	H II	10 18 17.0	+41 25 28	8.7	42	2000 Jan 8	804	39.8
							2000 Feb 3	1520	21.3
NGC 4102	Sb	H II/LINER	12 06 23.1	+52 42 39	17.0	82	2003 Apr 30	4014	4.9
NGC 4647	Sc	...	12 43 32.3	+11 34 55	16.8	81	2000 Apr 20	785	36.9
NGC 4713	Sd	LINER	12 49 57.9	+05 18 41	17.9	87	2003 Jan 28	4019	4.9
NGC 5457 ^c	Scd	...	14 03 12.6	+54 20 57	7.2	35	... ^c	... ^c	750

^aFrom NED.

^bFrom Tully (1988) except from Stetson et al. (1998) for NGC 5457.

^cNGC 5457 (M 101) was observed multiple times. The total observation time analyzed here is given in this table. The individual observations are listed in Table 3

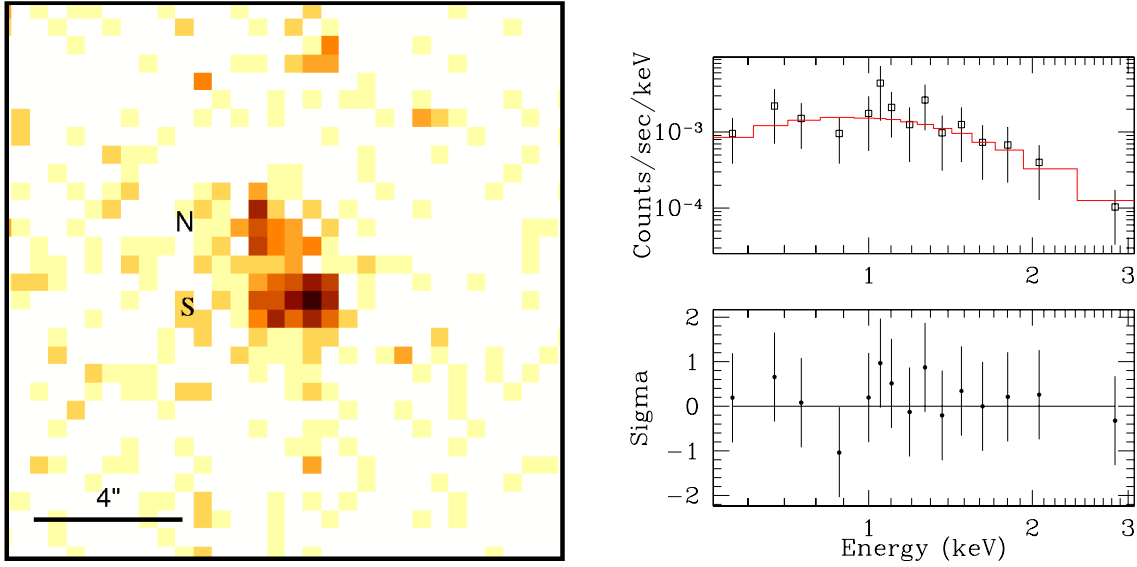


Fig. 2.— *Left*: Nucleus of NGC 3184, which appears to consist of two components, labeled N and S in the image. North is up and east to the left in the image. About 117 and 36 counts were detected in the southern and northern components, respectively. The image is $15''$ on a side. The black bar in the lower left represents a projected distance of $4''$, corresponding to ~ 170 pc. *Right*: Spectrum of the southern component of the nucleus of NGC 3184, together with an absorbed power-law model. Data points were binned so that there were at least 5 counts in each bin. The model shown above (red line) has $N_H = 3.0 \times 10^{21} \text{ cm}^{-2}$ and $\Gamma = 2.6$. The bottom panel shows the residuals.

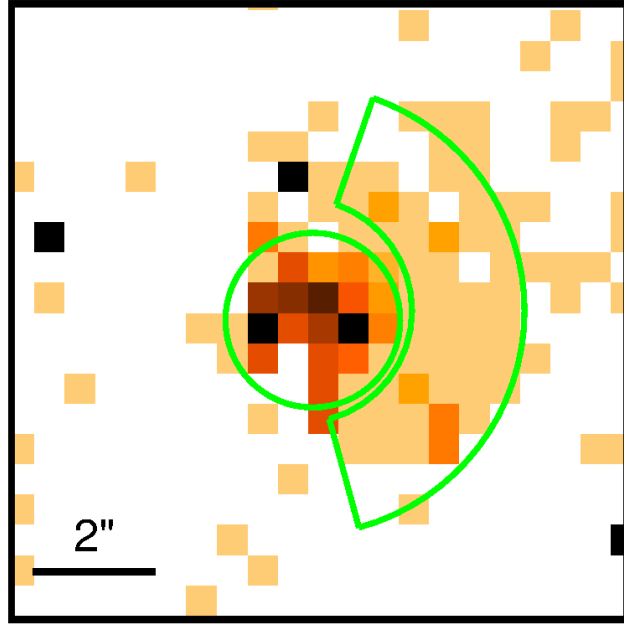


Fig. 3.— Nucleus of NGC 4102 with the regions used to extract counts overlaid on a hardness ratio map. North is up and east to the left in the image. The lightest colored pixels have $HR = -1$; the darkest pixels have $HR = +1$. The circle, 2.9 pixels in radius, was used for the core. The partial annulus is the region used to extract counts from the extended emission. The compact core has harder emission than the extended component. The bar on the lower left represents $2''$, or a projected distance of ~ 160 pc. The image is $10''$ on a side.

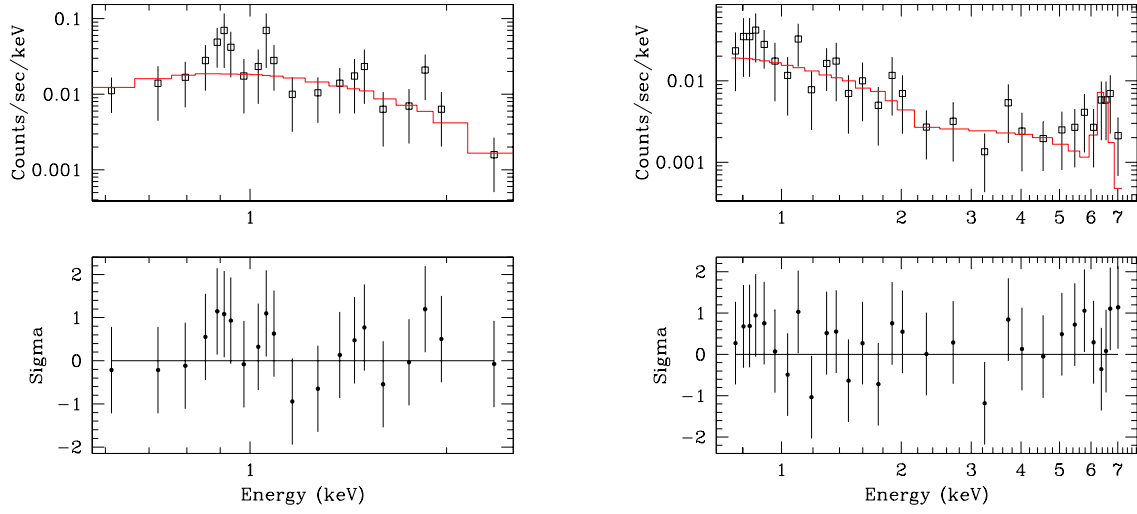


Fig. 4.— Spectra of NGC 4102. Data have been grouped to 5 counts per bin. *Left*: Spectrum of the extended component. The model is absorbed bremsstrahlung emission, with $N_H = (1.2^{2.8}_{-1.2}) \times 10^{21} \text{ cm}^{-2}$ and $kT = 1.2^{+8.6}_{-0.8} \text{ keV}$. *Right*: Spectrum of the core. The model is a reflected power-law and a Gaussian line, with no absorption in excess of Galactic. The best-fit parameters are $\Gamma \approx 2.3 \pm 0.6$ and reflection factor $R \approx 130$. The line was fixed at 6.4 keV with FWHM = 0.3 keV.

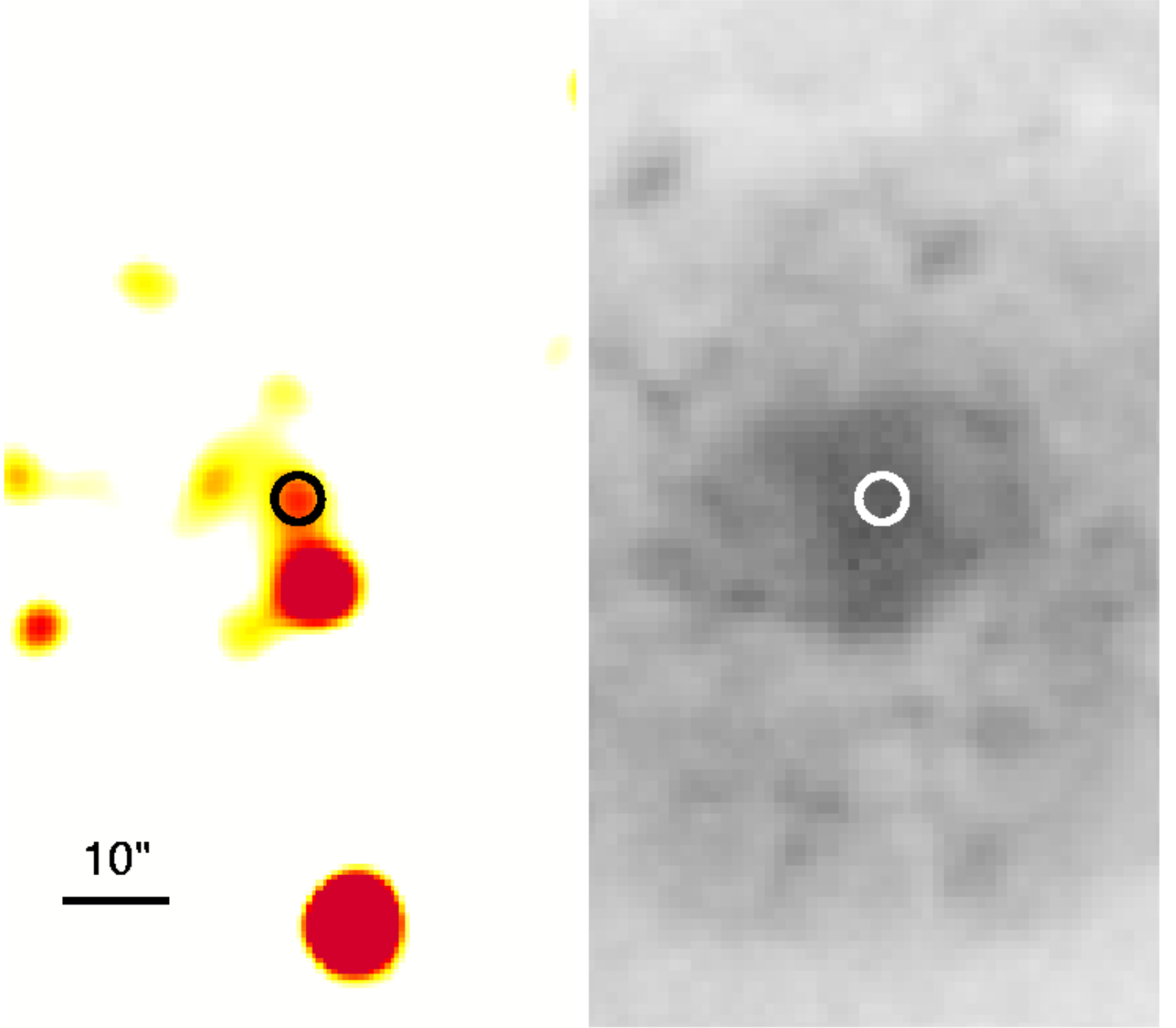


Fig. 5.— On the left are shown the residuals in the *Chandra* image after the elliptical galaxy NGC 4649 is modeled and subtracted. The residual image has been smoothed by convolving it with a Gaussian with $\sigma = 5$ pixels. The black circle, whose radius is $2.3''$ or roughly the 95% encircled-energy radius at 1.5 keV at that position, shows the probable nucleus of NGC 4647. On the right, a circle (white) of the same radius, whose center has the same celestial coordinates as the one on the left, is superposed on a DSS image of NGC 4647. Both images are shown on the same scale and have north up and east to the left. The bar in the lower left corresponds to $10''$, or a projected distance of ~ 800 pc.

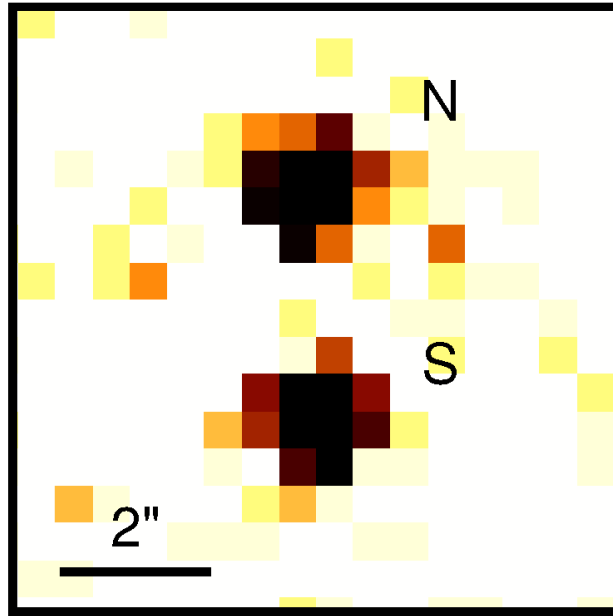


Fig. 6.— Nucleus of NGC 5457 (M 101). North is up and East to the left in the image. The nucleus is resolved into two sources, marked N and S in the image. The northern source N is the candidate active nucleus. The southern source S is a known star cluster (Pence et al. 2001). The black bar in the lower left represents a projected distance of $2''$, or ~ 70 pc. The image is $8''$ on a side.

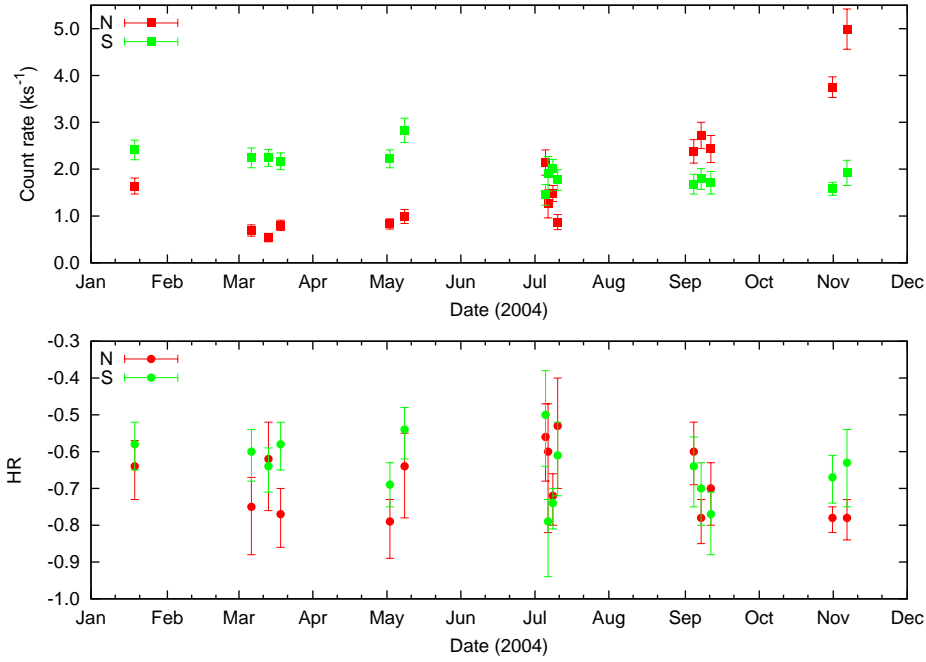


Fig. 7.— Variability and hardness ratio of the two M101 sources. Only observations performed in 2004 are shown here. The nucleus (source N) varies by a factor of ~ 9 between March and November. Uncertainty in count rate was derived assuming \sqrt{n} uncertainty in the counts.

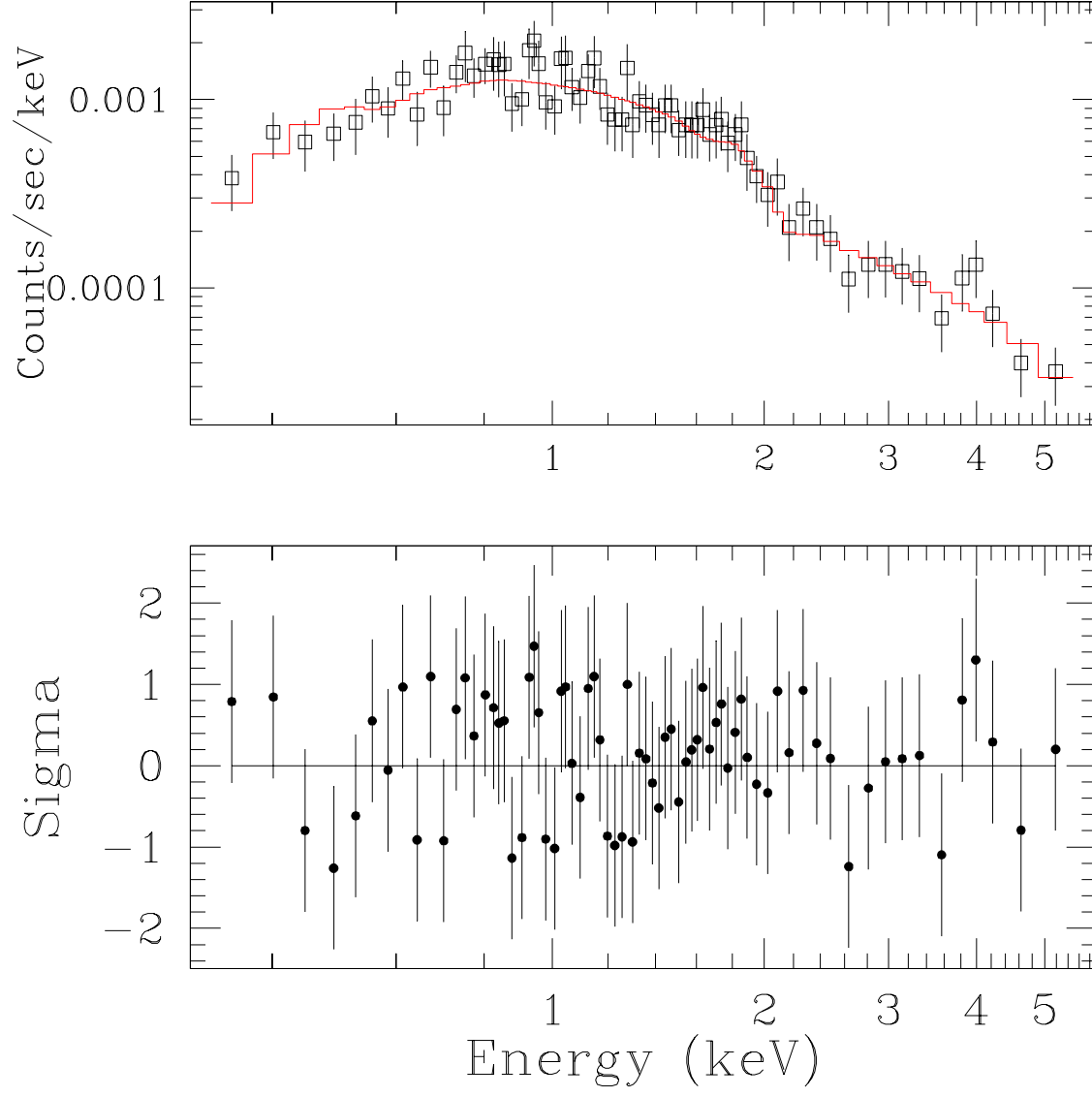


Fig. 8.— Spectrum of NGC 5457 obtained from merging all 2004 observations. Data have been binned to 15 counts per bin. The line shows the best fit model, an absorbed power-law ($\Gamma = 1.9$), thermal plasma ($kT = 0.44$ keV), and a line at ~ 4 keV. The lower panel shows the residuals.

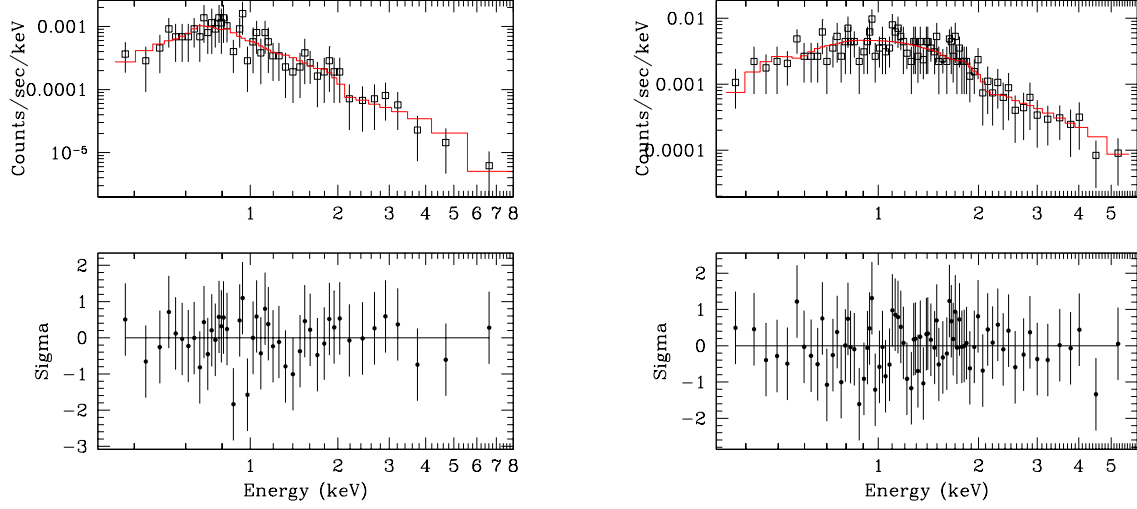


Fig. 9.— Spectrum of NGC 5457 in low and high states. Data have been binned to five counts per bin. *Left*: Low state spectrum. The best-fit model is a power-law plus MEKAL plasma with no absorption in excess of Galactic. *Right*: High state spectrum. The best-fit model is a power-law with both intrinsic and Galactic absorption but no plasma.

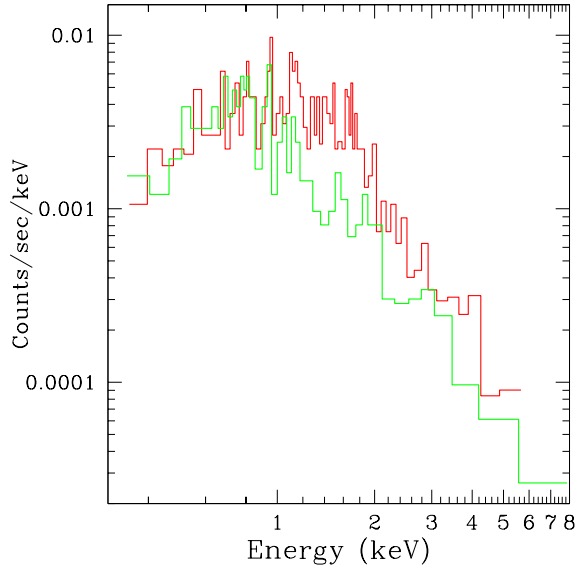


Fig. 10.— Spectrum of NGC 5457 in the high state (red) and the low state (green) overplotted.

Table 2. X-ray Measurements

Target	Counts						Bkg/Src Area Ratio	HR ^a
	Broad		Hard		Soft			
	Src	Bkg	Src	Bkg	Src	Bkg		
NGC 3169	159	23	148	5	11	18	21.4	+0.86 ^{+0.05} _{−0.03}
NGC 3184 N	36	95	4	33	32	62	92	−0.75 ^{+0.08} _{−0.13}
S	117	95	13	33	104	62	60	−0.77 ^{+0.05} _{−0.07}
NGC 4102 all	354	48	78	8	276	40	6.8	−0.55 ^{+0.04} _{−0.05}
core	171	48	68	8	103	40	52.5	−0.20 ^{+0.08} _{−0.07}
ext	115	48	6	8	109	40	26.1	−0.88 ^{+0.03} _{−0.06}
NGC 4647	15	38	1	15	14	23	10.1	−0.80 ^{+0.04} _{−0.20}
NGC 4713	10	4	1	0	9	4	21.4	−0.69 ^{+0.09} _{−0.25}
NGC 5457	314	256	23	45	291	211	20.8	−0.86 ± 0.03

^aHardness ratio, $HR = (H-S)/(H+S)$, where H and S are the counts in the hard and soft bands respectively, calculated using the method described in Park et al. (2006). The tool used is available at <http://hea-www.harvard.edu/AstroStat/BEHR/>.

Table 3. M101 X-ray Measurements

ObsID	Obs Date	Exp Time (ks)	North source			South source		
			Counts	Rate (ks ⁻¹)	HR	Counts	Rate (ks ⁻¹)	HR
934	2000 Mar 26	97.8	262	2.68	$-0.81^{+0.03}_{-0.04}$	264	2.70	-0.70 ± 0.04
4731 ^a	2004 Jan 19	56.2	92	1.64	$-0.64^{+0.07}_{-0.09}$	136	2.41	$-0.58^{+0.06}_{-0.07}$
5300	2004 Mar 7	52.1	36	0.69	$-0.75^{+0.08}_{-0.13}$	117	2.24	$-0.60^{+0.06}_{-0.08}$
5309	2004 Mar 14	70.8	38	0.54	$-0.62^{+0.10}_{-0.14}$	158	2.24	$-0.64^{+0.05}_{-0.07}$
4732	2004 Mar 19	69.8	56	0.80	$-0.77^{+0.07}_{-0.09}$	151	2.17	$-0.58^{+0.06}_{-0.07}$
5322	2004 May 3	64.7	54	0.83	$-0.79^{+0.06}_{-0.10}$	144	2.22	-0.69 ± 0.06
5323	2004 May 9	42.4	42	0.99	$-0.64^{+0.09}_{-0.14}$	120	2.83	$-0.54^{+0.06}_{-0.08}$
5338 ^a	2004 Jul 6	28.6	61	2.14	$-0.56^{+0.09}_{-0.12}$	41	1.45	$-0.50^{+0.12}_{-0.14}$
5339 ^b	2004 Jul 7	14.0	18	1.26	$-0.60^{+0.13}_{-0.22}$	27	1.90	$-0.79^{+0.06}_{-0.15}$
5340	2004 Jul 9	54.4	81	1.48	$-0.72^{+0.06}_{-0.08}$	110	2.02	$-0.74^{+0.04}_{-0.07}$
4734	2004 Jul 11	35.5	31	0.87	$-0.53^{+0.13}_{-0.17}$	63	1.77	$-0.61^{+0.09}_{-0.11}$
6114	2004 Sep 5	38.2	91	2.38	$-0.60^{+0.08}_{-0.09}$	64	1.68	$-0.64^{+0.08}_{-0.11}$
6115	2004 Sep 8	35.4	96	2.72	$-0.78^{+0.05}_{-0.07}$	63	1.79	$-0.70^{+0.07}_{-0.10}$
4735	2004 Sep 12	28.8	70	2.43	$-0.70^{+0.07}_{-0.10}$	49	1.71	$-0.77^{+0.06}_{-0.11}$
4736 ^{a b}	2004 Nov 1	77.4	290	3.75	$-0.78^{+0.03}_{-0.04}$	122	1.58	$-0.67^{+0.06}_{-0.07}$
6152 ^a	2004 Nov 7	26.7	133	4.99	$-0.78^{+0.05}_{-0.06}$	51	1.92	$-0.63^{+0.09}_{-0.12}$

^aSource extended, or possibly image smeared.

^bPossible residual contamination from background flare.

Table 4. X-Ray Spectral Fits

Target	Galactic	Model ^a	Spectral Fit Parameters						$\chi^2_{\nu}(\text{dof})$
	N_{H} (10^{20} cm^{-2})		kT (keV)	N_{H} (10^{21} cm^{-2})	Γ	Refl. ^b	Line (keV)	EW (keV)	
NGC 3169	2.86	ab(p1)	...	99^{+46}_{-36}	$2.0^{+1.2}_{-1.1}$	$1.1(26)^{\text{c}}$
		ab(p1)	...	116^{+90}_{-52}	$2.6^{+2.1}_{-1.5}$	$0.3(22)$
NGC 4102 core	1.79	ab(p1)	...	$0^{+1.4}$	2.0 ± 0.5	$7.4(27)^{\text{c}}$
		ab(rn)	...	$0^{+0.4}$	1.8 ± 0.4	108^{+149}_{-61}	$2.3(26)^{\text{c}}$
		ab(rn+g)	...	$0^{+1.9}$	$2.3^{+0.6}_{-0.5}$	129 ^d	6.4	3.3	$0.6(25)$
		ab(rn+g)	...	$0^{+0.6}$	$2.2^{+0.6}_{-0.5}$	129^{+283}_{-85}	6.4	2.5	$1.6(25)^{\text{c}}$
		ab(br)	$1.2^{+8.6}_{-0.8}$	$1.2^{+2.8}_{-1.2}$	$0.5(18)$
NGC 5457 sep. low	1.15	ab(me+p1)	$0.3^{+0.2}_{-0.1}$	$0^{+1.8}$	1.7 ± 0.5	$0.5(28)$
sep. high		ab(p1)	...	$1.5^{+1.1}_{-1.5}$	$2.2^{+0.4}_{-0.3}$	$0.5(40)$
sim. low		ab(me+p1)	$0.3^{+0.3}_{-0.1}$	$0.42^{+1.9}_{-0.42}$	$2.0^{+0.4}_{-0.2}$	$0.5(28)$
sim. high		ab(p1)	...	1.1 ± 0.6	$2.0^{+0.4}_{-0.2}$	$0.5(41)$
merged		ab(p1)	...	0.6 ± 0.4	1.9 ± 0.2	$0.6(70)$

^aModel labels: **ab**=**xswabs**, photoelectric absorption; **ga**=**xswabs** with value frozen at Galactic column density towards this target; **br**=**xsbremss**, thermal bremsstrahlung; **g**=**gauss1d**, one-dimensional Gaussian; **me**=**xsmekal**, thermal plasma; **p1**=**powlaw1d**, one-dimensional power law; **rn**=**xspexrav**, power-law reflected by neutral material.

^bReflection scaling factor.

^cCash statistic (**cstat** in *Sherpa*).

^dUnconstrained by fit.

Table 5. Inferred nuclear luminosities

	Filter or Band	NGC 3169 (Sa)	NGC 4102 (Sb)	NGC 4647 (Sc)	NGC 3184 (Scd)	NGC 5457 (Scd)	NGC 4713 (Sd)
X-ray	0.3–8 keV	41.7	40.2	39.0 ^{ab}	37.3 ^c	37.5–38.5 ^d	38.6 ^c
UV & Opt.	F300W	< 39.4
	F336W	39.0	...
	F547M	39.5	...
	F606W	39.5	...	40.1
IR	K_s	42.6	42.8	38.8	40.9	41.0	41.0
Radio	15 GHz	< 36.8
	5 GHz	37.2	< 35.8	...
	1.4 GHz	...	36.0	36.9 ^b	< 35.1	< 34.9	< 35.7

Note. — Values are $\log(L/\text{erg s}^{-1})$ in the specified bandpass in the x-ray and $\log(\nu L_\nu/\text{erg s}^{-1})$ where a single filter, wavelength, or frequency is given. Note that the values are derived from observations with varied instruments, PSFs, apertures, and signal-to-noise ratios, and the uncertainties can be as large as a factor of two.

^a0.3–12 keV.

^bLarge positional uncertainty makes it unclear whether the detected source is really the nucleus.

^cBased on a small number of counts. A power-law spectrum was assumed. Intrinsic absorption is unknown.

^dVariable source.

- Space Telescope Science Institute, Baltimore, Maryland, October 17 and 18, 2002.
Edited by Santiago Arribas, Anton Koekemoer, and Brad Whitmore. Baltimore, MD:
Space Telescope Science Institute, 2002., p.301, ed. S. Arribas, A. Koekemoer, &
B. Whitmore
- Dong, X. Y., & De Robertis, M. M. 2006, *AJ*, 131, 1236
- Dudik, R. P., Satyapal, S., Gliozzi, M., & Sambruna, R. M. 2005, *ApJ*, 620, 113
- Eracleous, M., Livio, M., & Binette, L. 1995, *ApJ*, 445, L1
- Ferrarese, L. 2002, *ApJ*, 578, 90
- Ferrarese, L., & Merritt, D. 2000, *ApJ*, 539, L9
- Fiore, F. et al. 2003, *A&A*, 409, 79
- Freedman, W. L. et al. 2001, *ApJ*, 553, 47
- Ganda, K., Falcón-Barroso, J., Peletier, R. F., Cappellari, M., Emsellem, E., McDermid,
R. M., de Zeeuw, P. T., & Carollo, C. M. 2006, *MNRAS*, 367, 46
- Gebhardt, K. et al. 2000, *ApJ*, 539, L13
- Ghosh, H., Pogge, R. W., Mathur, S., Martini, P., & Shields, J. C. 2007, *ApJ*, 656, 105
- Graham, A. W., Driver, S. P., Allen, P. D., & Liske, J. 2007, *MNRAS*, 378, 198
- Graham, A. W., Erwin, P., Caon, N., & Trujillo, I. 2001, *ApJ*, 563, L11
- Greene, J. E., & Ho, L. C. 2004, *ApJ*, 610, 722
- Hasinger, G., Miyaji, T., & Schmidt, M. 2005, *A&A*, 441, 417
- Heckman, T. M. 1980, *A&A*, 87, 152
- Heckman, T. M., Kauffmann, G., Brinchmann, J., Charlot, S., Tremonti, C., & White,
S. D. M. 2004, *ApJ*, 613, 109
- Héraudeau, P., & Simien, F. 1998, *A&AS*, 133, 317
- Ho, L. C., Filippenko, A. V., & Sargent, W. L. W. 1997, *ApJS*, 112, 315
- Holtzman, J. A. et al. 1995, *PASP*, 107, 156
- Howarth, I. D. 1983, *MNRAS*, 203, 301

- Kennicutt, Jr., R. C. et al. 2003, *PASP*, 115, 928
- Kormendy, J., & Richstone, D. 1995, *ARA&A*, 33, 581
- Kotanyi, C. G. 1980, *A&AS*, 41, 421
- Laor, A. 2003, *ApJ*, 590, 86
- Larsen, S. S. 2004, *A&A*, 416, 537
- Leitherer, C. et al. 1999, *ApJS*, 123, 3
- Levenson, N. A., Heckman, T. M., Krolik, J. H., Weaver, K. A., & Życki, P. T. 2006, *ApJ*, 648, 111
- Marconi, A., & Hunt, L. K. 2003, *ApJ*, 589, L21
- Marconi, A., Risaliti, G., Gilli, R., Hunt, L. K., Maiolino, R., & Salvati, M. 2004, *MNRAS*, 351, 169
- Martini, P., Boeker, T., & Schinnerer, E. 2008, *ApJ*, in prep
- Martini, P., Kelson, D. D., Mulchaey, J. S., & Trager, S. C. 2002, *ApJ*, 576, L109
- McElroy, D. B. 1995, *ApJS*, 100, 105
- McLure, R. J., & Dunlop, J. S. 2001, *MNRAS*, 327, 199
- McLure, R. J., Willott, C. J., Jarvis, M. J., Rawlings, S., Hill, G. J., Mitchell, E., Dunlop, J. S., & Wold, M. 2004, *MNRAS*, 351, 347
- Merloni, A. 2004, *MNRAS*, 353, 1035
- Nagar, N. M., Falcke, H., & Wilson, A. S. 2005, *A&A*, 435, 521
- Nicastro, F. 2000, *ApJ*, 530, L65
- Nicastro, F., Martocchia, A., & Matt, G. 2003, *ApJ*, 589, L13
- Park, T., Kashyap, V. L., Siemiginowska, A., van Dyk, D. A., Zezas, A., Heinke, C., & Wargelin, B. J. 2006, *ApJ*, 652, 610
- Pence, W. D., Snowden, S. L., Mukai, K., & Kuntz, K. D. 2001, *ApJ*, 561, 189
- Peterson, B. M. et al. 2005, *ApJ*, 632, 799

- Pounds, K. A., Reeves, J. N., Page, K. L., & O’Brien, P. T. 2004, *ApJ*, 605, 670
- Prestwich, A. H., Irwin, J. A., Kilgard, R. E., Krauss, M. I., Zezas, A., Primini, F., Kaaret, P., & Boroson, B. 2003, *ApJ*, 595, 719
- Randall, S. W., Sarazin, C. L., & Irwin, J. A. 2006, *ApJ*, 636, 200
- Shankar, F., Salucci, P., Granato, G. L., De Zotti, G., & Danese, L. 2004, *MNRAS*, 354, 1020
- Skrutskie, M. F. et al. 2006, *AJ*, 131, 1163
- Snellen, I. A. G., Lehnert, M. D., Bremer, M. N., & Schilizzi, R. T. 2003, *MNRAS*, 342, 889
- Soria, R., Baldi, A., Risaliti, G., Fabbiano, G., King, A., La Parola, V., & Zezas, A. 2007, *MNRAS*, 379, 1313
- Stetson, P. B., et al. 1998, *ApJ*, 508, 491
- Stobart, A.-M., Roberts, T. P., & Wilms, J. 2006, *MNRAS*, 368, 397
- Terashima, Y., & Wilson, A. S. 2003, *ApJ*, 583, 145
- Tully, R. B. 1988, *Nearby galaxies catalog* (Cambridge and New York, Cambridge University Press, 1988, 221 p.)
- Ulvestad, J. S., & Ho, L. C. 2002, *ApJ*, 581, 925
- Vázquez, G. A., & Leitherer, C. 2005, *ApJ*, 621, 695
- Walcher, C. J. et al. 2005, *ApJ*, 618, 237
- Williams, R. J., Mathur, S., & Pogge, R. W. 2004, *ApJ*, 610, 737
- Willis, A. G., Oosterbaan, C. E., & de Ruiter, H. R. 1976, *A&AS*, 25, 453
- Young, A. J., Nowak, M. A., Markoff, S., Marshall, H. L., & Canizares, C. R. 2007, *ApJ*, 669, 830

Table 6. NGC 3184 nuclear luminosity in *Spitzer* bands

Band (μm)	Aperture Radius	$\log(\nu L_\nu)$ (erg s^{-1})
3.6	3''	40.6
4.5	3''	40.4
5.8	3''	40.7
8.0	3''	40.8
24	6''	41.1
70	10''	41.5
160	10''	41.7